

MULTISCALE DATA INTEGRATION USING COARSE-SCALE MODELS *

Y. EFENDIEV[†], AND , A. DATTA-GUPTA[‡], AND , I. OSAKO[§], AND , AND B. MALLICK[¶]

Abstract.

In this paper we combine a novel multiscale data integration technique introduced in [16] with upscaling techniques for spatial modeling of permeability. The approach introduced in the paper is hierarchical and the conditional information from different length scales is incorporated into the posterior distribution using a Bayesian framework. Because of a complicated structure of the posterior distribution Markov Chain Monte Carlo (MCMC) based approaches are used to draw samples of the fine-scale permeability field.

1. Introduction. With the increasing interest in accurate prediction of subsurface properties, subsurface characterization based on limited dynamic data, such as production and pressure transient data, as well as static data takes on greater importance. Uncertainties on the detailed description of reservoir lithofacies, porosity, and permeability are large contributors to uncertainty in reservoir performance forecasting. Reducing this uncertainty can be achieved by integrating additional data in subsurface modeling. In general, we have static data such as well logs, cores, seismic traces, and dynamic data such as multiphase production history, pressure transient tests and tracer tests etc. Integration of the data from different sources is a nontrivial task because different data sources scan different length scales of heterogeneity and can have different degree of precision. For example, well logs can resolve heterogeneity at the scale of a few feet whereas production data usually scan the length scales comparable to the inter-well distances.

In previous findings several methods have been introduced which incorporate multiscale data with a primary focus on integrating seismic and well data. These methods include conventional techniques such as cokriging and its variations [5, 21, 22, 13], Sequential Gaussian Simulation with Block Kriging [1], and Bayesian updating of point kriging [1, 6]. Most kriging-based methods are restricted to multi-Gaussian and stationary random fields [5, 21, 22, 13, 1, 6, 4]. Thus, they require variogram construction which can be difficult because of limited data set. Improper variograms can lead to errors and inaccuracies in the estimation. Thus, one might also need to consider the uncertainty in the variogram models during the estimation [7]. Furthermore, most of the multiscale integration algorithms assume a linear relationship between the scales [16].

The goal of this paper is to combine a novel multiscale data integration technique introduced in [16] with accurate upscaling techniques for spatial modeling of permeability in petroleum reservoirs. Reservoir properties such as permeability data may be available at various scales. The fine-scale data represents point measurements such as well logs and cores. The coarse-scale data reflect the effects of the heterogeneities of the fine-scale permeability field and may be obtained based on production and/or seismic data. Such coarse-scale information will typically be associated with higher precision compared to the fine-scale data. In this paper we propose an approach to spatial modeling of permeability conditioned on coarse-scale measurements and some fine-scale conditioning points. We employ a Bayesian framework and assume that the fine-scale permeability distribution can be represented by a Markov Random Field. Bayesian approaches allow us to formulate a posterior distribution of the fine-scale permeability field in terms of the coarse measurements. The likelihood function in this posterior distribution describes the stochastic link between the coarse-scale and the fine-scale permeability data. To calculate these kinds of likelihood functions we use upscaling procedures that involve the local solutions of the flow equation. Upscaling operators introduced in this way are nonlocal and, thus, the obtained posterior distributions are non-explicit. To draw the permeability from the posterior distribution rejection sampling or importance sampling can be used, but due to complicated structure of the posterior distribution they may be very inefficient. In this paper, Markov Chain Monte Carlo (MCMC) ([14]) based approaches are mainly used. The main idea of MCMC is create Markov Chain

*This work is supported by NSF grant DMS-0327713

[†]Department of Mathematics, Texas A&M University, College Station, TX 77843

[‡]Department of Petroleum Engineering, Texas A&M University, College Station, TX 77843

[§]Department of Petroleum Engineering, Texas A&M University, College Station, TX 77843

[¶] Department of Statistics, Texas A&M University, College Station, TX 77843

with some proper choice of transition matrix such that the stationary distribution of the chain becomes the posterior distribution of the permeability field.

Some representative numerical examples are presented in the paper. For the first set of numerical examples the coarse-scale permeability field is computed using a reference true fine-scale permeability field. Using only the coarse-scale permeability and few sampling points for the fine-scale permeability field we sample the fine scale permeability field from the posterior distribution. The coarse-scale permeability field is not imposed exactly in the likelihood function for the following two reasons. First, in practice the coarse-scale permeability fields are often obtained from indirect information, for example seismic data that are affected by noise or artifacts or correlations that may have large scatter. The second reason for not imposing coarse-scale permeabilities exactly is due to the fact that the inversion of the production data on the coarse grid does not take into account the adequate form of the coarse-scale models. Indeed, the inversion on the coarse grid for flow problems often involves the same flow equations as the underlying fine ones, for example, the same relative permeabilities are used for the coarse-scale problems as those for the fine scale problems or the effects of macrodispersion are neglected. It is known that [9, 11, 10, 12] the flow equations at the coarse level may have different form from the underlying fine-scale equations. In general this form depends on the detail nature of the heterogeneities which are very difficult to obtain in solving inverse problems. Thus, calculating the coarse grid permeability fields by matching the production history introduces some errors. Since it is very difficult to assess these kinds of errors in general, we impose the coarse-scale permeability field with some precision. In the first set of numerical examples, we study the various degrees of coarsening and precisions for the coarse-scale fields. For the second set of our numerical examples we use the coarse-scale production data calculated from the inversion of the production data in [16] with 15 injectors and 27 producers. Two coarse-scale data, medium scale and large scale, are considered. We compare the production histories in the producing wells.

Finally, in the paper we study the effects of upscaling errors on the posterior distribution. The upscaling procedures, in general, involve inaccuracies due to the multiscale nature of the underlying fine-scale permeability field. In Appendix, we study the effects of upscaling errors on the posterior distribution.

2. Methodology. In this section we discuss the Bayesian framework used in generating the realizations of fine-scale permeability field conditioned on a coarse-scale permeability data and some sampling points. Fine-scale permeability field is assumed to be represented by a Markov Random Field. We assume that k_1, k_2, \dots, k_N are permeability fields at different scales (1 - finest (or, simply, fine), N -coarsest). Using Bayes theorem we have

$$P(k_1, \dots, k_N) = P(k_1)P(k_2|k_1)P(k_3|k_1, k_2) \cdots P(k_N|k_1, k_2, \dots, k_{N-1}), \quad (2.1)$$

where $P(k_{i+1}|k_1, \dots, k_i)$ represents the conditional distributions of permeability field at $i+1$ coarse level with respect to that at levels 1 to i , $P(k_1, \dots, k_N)$ represents the joint probability distributions and $P(k_1)$ represents the probability distribution of the fine-scale permeability field. We assume that $P(k_i|k_{i-1}, \dots, k_1) = P(k_i|k_1)$, i.e., the coarse-scale permeabilities depend on each other via the finest scale permeability field. For further calculations the probability distribution of the fine-scale permeability will be assumed to be known. In particular, $P(k_1)$ will be taken to be a Gaussian Markov Random Field which is introduced later. From (2.1) we have

$$P(k_1|k_2, \dots, k_N) = \frac{P(k_1, \dots, k_N)}{P(k_2, \dots, k_N)} = \frac{P(k_1)P(k_2, \dots, k_N|k_1)}{P(k_2, \dots, k_N)} \propto P(k_1)P(k_2, \dots, k_N|k_1). \quad (2.2)$$

The equation (2.2) can be generalized to consider some observed data at sparse fine-scale locations. Denote by k_1^o observed fine-scale data and k_1^u unknown values of the fine-scale permeability that need to be generated. Then the equation (2.2) can be generalized to

$$P(k_1^u|k_1^o, k_2, \dots, k_N) \propto P(k_2|k_1)P(k_3|k_1) \cdots P(k_N|k_1)P(k_1^u|k_1^o) \quad (2.3)$$

where $k_1 = \{k_1^u, k_1^o\}$. The prior distribution of k_1 may involve parameters with uncertainties, such as variance etc. One can similarly write down the conditional distributions with respect to these parameters.

2.1. Gaussian MRF. In this paper we will use Gaussian MRF for prior distributions though the procedure can be extended to more general random fields. Gaussian MRF specifies the conditional probability of fine-scale permeability field at the location i to be normally distributed with a mean that depends on the elements of its neighborhood, denoted by \mathcal{N}_i . The neighborhood can be chosen in different ways including nearest neighbors or neighbors along some direction if the field is anisotropic. The conditional distribution of Gaussian MRF is given by

$$P(k_1(x_i)|k_1(x_j), j \in \mathcal{N}_i) = \frac{1}{\sqrt{2\pi\sigma^2}} \exp\left(-\frac{1}{2\sigma^2}(k_1(x_i) - \sum_{j \in \mathcal{N}_i} w_{ij}k_1(x_j))^2\right), \quad (2.4)$$

where w_{ij} are weights corresponding to the neighbors of the location x_i , and x_i and x_j are the physical locations of the fine-scale field. (2.4) leads to the following joint distributions

$$P(k_1) = \frac{1}{\sqrt{(2\pi\sigma^2)^n}} \det(W)^{1/2} \exp\left(-\frac{1}{2\sigma^2}k_1^T W k_1\right),$$

where W is $n \times n$ weight matrix whose diagonal elements are unity and off-diagonal elements are $-w_{ij}$ specified such that W is positive semi-definite matrix. Variance σ in our studies is assumed to depend on the neighbors. The latter is more appropriate for heterogeneous fields. In particular, we assume

$$P(k_1(x_i)|k_1(x_j), j \in \mathcal{N}_i) \propto \theta^{1/2} \exp\left(-\frac{1}{2}\theta \sum_{j \in \mathcal{N}_i} \beta_{ij}(k_1(x_i) - k_1(x_j))^2\right).$$

β_{ij} are prescribed in the following way. $\beta_{ij} = 0$ unless x_i and x_j are neighbors, otherwise specified numbers for the neighbors are prescribed. The choice of β_{ij} allows us to incorporate the prior knowledge. The simplest choice will be $\beta_{ij} = 1$ if x_i and x_j are neighbors. One can choose β_{ij} to reproduce global spatial properties such prior covariance or variogram. More discussion along these lines can be found in [17]. Finally, we would like to note that one can easily incorporate anisotropy in spatial properties by an appropriate choice of the neighborhood set.

2.2. Linking two different scales. In most practical situation we deal at most with three different scales, though one can introduce various coarse-scales, for example, based on production data. The link between the coarse and the fine-scale levels are usually nontrivial because one needs to take into account the effects of all the scales present at the fine level. In the past simple arithmetic, harmonic or power averages have been used to link properties at various scales. These averages can be reasonable for low heterogeneities or for volumetric properties such as porosity. For permeabilities, simple averaging can lead to inaccurate and misleading results. In this paper we use the upscaling methods based on local solution of the equations, [8, 20].

Consider the fine-scale permeability that is defined in the domain with underlying fine grid as shown in Figure 2.1. On the same graph we illustrate a coarse-scale partition of the domain. To calculate the coarse scale permeability field at this level we need to determine it for each coarse block, K . The coarse block permeability can be defined both using the solutions of local or global problems. The main idea of the calculation of a coarse-scale permeability is that it delivers the same average response as that of the underlying fine-scale problem locally. The calculation of the coarse-scale permeability based on local solutions is schematically depicted in Figure 2.1. For each coarse domain K we solve the local problems

$$\text{div}(k_1(x)\nabla\phi_i) = 0, \quad (2.5)$$

with some boundary conditions such that $\frac{1}{|K|} \int_K \nabla\phi_i = -e_i$, where e_i is the unit vector in the i direction. Here $k_1(x)$ denotes the fine-scale permeability field. One of such boundary conditions are given by $\phi_1 = 1$ and $\phi_i = 0$ on the opposite sides along the direction e_i and no flow boundary conditions on all other sides. Then the coarse-scale permeability is given by

$$(k_i(x)e_m, e_l) = \frac{1}{|K|} \int_K (k_1(x)\nabla\phi_m(x), e_l)dx, \quad (2.6)$$

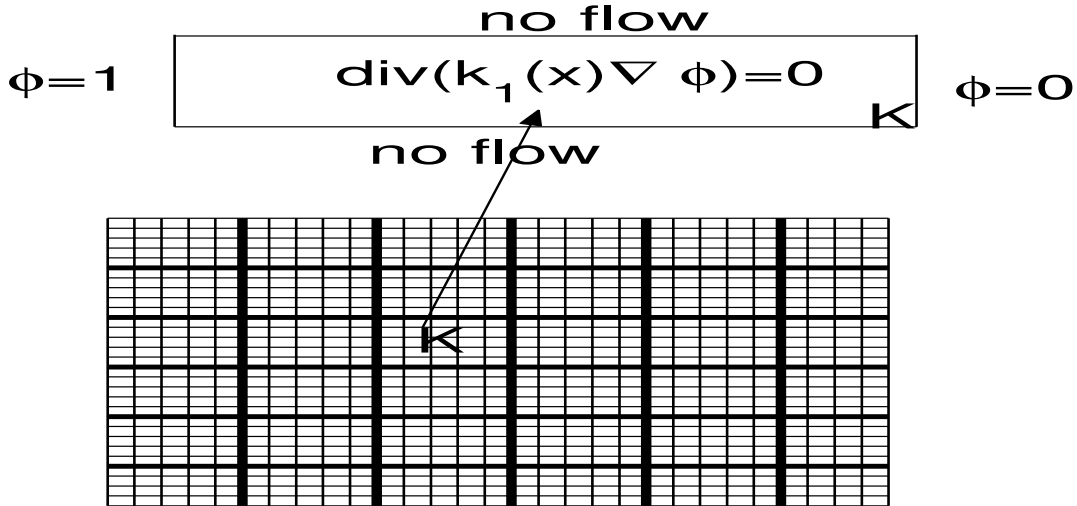


FIG. 2.1. Schematic description of the upscaling

i.e., the coarse-scale permeability fields gives the same average response as the underlying fine-scale one. Various boundary condition can have some influence on the accuracy of the calculations, including periodic, Dirichlet and etc. These issues have been discussed in [20]. In particular, for determining the coarse-scale permeability field one can choose the local domains that are larger than target coarse block, K , for (2.5). Further (2.6) is used in the domain K , where ϕ_m are computed in the larger domains with correct scaling (see [20]). This way one reduces the effects of the artificial boundary conditions imposed on K . These issues have been also discussed, for example, in [20]. All upscaling procedures introduce some errors. The question arises: how do upscaling errors influence the posterior distribution? The convergence results for the upscaled quantities can be obtained under the assumption of scale separation. In Appendix we study the convergence of posterior distributions when some convergence for the upscaled models are known.

The use of the local solutions (2.5) for determining the permeability field at different scales gives non-explicit relation for conditional distribution. $P(k_i|k_1)$ is defined via the solutions of (2.5) which takes into account the local heterogeneities. For further discussion we denote by \mathcal{L}_i the local operator that maps the local fine-scale permeability field k_1 into k_i . For our computations we assume

$$k_i = \mathcal{L}_i(k_1) + \epsilon_i, \quad (2.7)$$

where ϵ_i are some random fluctuations that represent inaccuracies in the coarse-scale permeability. One of the sources of these fluctuations are the errors associated with the solving inverse problems on the coarse grid. The other source of the inaccuracies of measured coarse-scale permeability is due to the fact that the inversion on the coarse grid does not take into account the adequate form of the coarse-scale models. Indeed, the inversion on the coarse grid for flow problems often involves the same flow equations as the underlying fine ones, for example, the same relative permeabilities are used for the coarse-scale problems as those for the fine scale problems or the effects of macrodispersion are neglected. It is known that [9, 11, 10, 12] the flow equations at the coarse level may have different form from the underlying fine-scale equations. In general this form depends on the detail nature of the heterogeneities which are very difficult to obtain in solving inverse problems. Thus, calculating the coarse grid permeability fields by matching the production history introduces some errors. Since it is very difficult to assess these kinds of errors in general we use Gaussian noise in (2.7).

2.3. MCMC approach. The posterior distribution is given by

$$P(k_1^u|k_1^o, k_2, \dots, k_N) \propto P(k_1^u|k_1^o)P(k_2|k_1)P(k_3|k_1) \cdots P(k_N|k_1), \quad (2.8)$$

where k_1^u and k_1^o are unobserved and observed data. k_i and k_1 are linked through the solution of the local partial differential equations. We can generate multiple realizations from this posterior distribution using Markov Chain Monte Carlo (MCMC). This approach is known to be very general and can handle complex posterior distributions as the ones considered here. The main idea of MCMC is the use of Markov Chain with a specified stationary distribution. The random drawing from the target distribution can be accomplished by a sequence of draws from full conditional distribution. Since the full conditionals have non-explicit form involving \mathcal{L} Metropolis-Hastings algorithm is used.

For our numerical examples we consider only two or three scales. In the case of two scales, we have

$$P(k_1^u|k_1^o, k_2) \propto P(k_1^u|k_1^o)P(k_2|k_1^u, k_1^o).$$

The full conditional is given by

$$P(k_1(x_i)|k_1(x_j), k_2(x_l)) \propto \theta^{1/2} \exp\left(-\frac{1}{2} \sum_{j \in \mathcal{N}_i} \beta_{ij} (k_1(x_i) - k_1(x_j))^2\right) \frac{1}{\sigma_2 \sqrt{2\pi}} \exp\left(-\frac{1}{2\sigma_2^2} (k_2(x_l) - \mathcal{L}_2^K(k_1))^2\right), \quad (2.9)$$

where \mathcal{L}_2^K denotes the operator that maps the fine-scale information of the permeability field to the coarse-scale permeability field, K is the coarse block corresponding to the fine site i and l is the global index of the coarse block K , $k_2(x)|_K = k_2(x_l)$. For the case of n scales the posterior distribution has the following form

$$P(k_1(x_i)|k_1(x_j), k_2, \dots, k_N) \propto \theta^{1/2} \exp\left(-\frac{1}{2} \sum_{j \in \mathcal{N}_i} \beta_{ij} (k_1(x_i) - k_1(x_j))^2\right) \frac{1}{\sigma_2 \sqrt{2\pi}} \exp\left(-\frac{1}{2\sigma_2^2} (k_2 - \mathcal{L}_2^K(k_1))^2\right) \dots \frac{1}{\sigma_N \sqrt{2\pi}} \exp\left(-\frac{1}{2\sigma_N^2} (k_N - \mathcal{L}_N^K(k_1))^2\right). \quad (2.10)$$

As before, we assume that the coarse-scale permeability fields are defined

$$k_i|_K = \mathcal{L}_i^K(k_1) + \epsilon_i, \quad (2.11)$$

where $\epsilon_i \sim N(0, \sigma_i^2)$. By choosing σ_i very small we impose the coarse-scale constraint exactly which is called hard constraint. As we discussed above the hard constraint is not suitable for our computations because of the inaccuracies in the calculations of the coarse-scale permeability fields.

MCMC scheme is carried out by updating each $k_1(x_i)$ using Metropolis-Hasting step. In the single step of Metropolis-Hasting algorithm, each candidate, $k_1(x_i)^*$ is generated from a pre-specified proposal distribution. Assuming a symmetric proposal distribution, a candidate $k_1(x_i)^*$ is accepted with a probability $q(k_1(x_i), k_1^*(x_i))$,

$$q(k_1(x_i), k_1^*(x_i)) = \min\left(1, \frac{P(k_1^*(x_i)|k_1^*(x_i), k_2, \dots, k_N)}{P(k_1(x_i)|k_1(x_i), k_2, \dots, k_N)}\right).$$

3. Numerical Results. For our first numerical test a 40×40 reference field (see left plot of Figure 3.1) is chosen as a true field. This field is obtained by GMRF described earlier. The spatial interaction coefficients are chosen $\beta = 1$ for all the neighbors. We pick only three points near left bottom corner and right upper corner (the well locations) as the fine-scale sampling points. The coarse-scale permeability field is calculated using the upscaling procedure described earlier on 10×10 coarse grid. As for the precision of the coarse scale data (see (2.11)) we assign $\sigma = 0.1$. Next based on the values of the fine-scale permeability field at the sampling points and the coarse-scale block values we simulate the realizations of the fine-scale permeability field from the posterior distribution. In Figure 3.1 (right plot) we plot a realization of the simulated field. We discard first 10000 iterations as burn-in iterations for MCMC. From this figure one

can observe a good agreement with the true fine-scale data (left figure of Figure 3.1). One of the reasons for the good agreement is that the coarse scale data is sufficiently fine and each coarse block has 4×4 resolution. In the Figure 3.2 we plot both the coarse-scale permeability field as well as cross-plot between the coarse-scale permeability fields obtained from the simulated and true fine-scale permeability fields. Since the precision is chosen to be small the coarse-scale data obtained from our simulated fine-scale data is close to the coarse-scale data corresponding to the true field. For illustration purposes all permeability fields are interpolated onto 400×400 grid before plotting. The latter allows to see the structure of the permeability field more clearly. This interpolation is done only for visualization purposes. For our next numerical example we compare the fractional flow curves corresponding to the true and simulated fine-scale permeability fields that are depicted in Figure 3.3 using single phase flow simulations,

$$\begin{aligned} -\operatorname{div}(k\nabla p) &= 0, & v &= -k\nabla p \\ \frac{\partial S}{\partial t} + v\nabla S &= 0. \end{aligned} \tag{3.1}$$

The boundary conditions are chosen such that flow is driven from the lower left corner of the model to the upper right corner. This is achieved by specifying $p = 1$, $S = 1$ along the $x = 0$ edge for $0 \leq z \leq 0.1$ and $p = 0$ along the $x = 1$ edge for $0.9 \leq z \leq 1$. Results are presented in terms of the fraction of the produced fluid (designated F , where $F = q_o/q$, with q_o the volumetric flow rate of oil produced at the outlet edge and q the total flow rate of the fluid produced at the outlet edge) versus pore volumes injected (PVI). PVI is analogous to dimensionless time and is defined as qt/V_p , where t is dimensional time and V_p is the total pore volume of the system. The transport equations is discretized using second order minmod schemes. We see from the Figure 3.3 that the simulations with the fine-scale permeability field that is computed using our method tracks the true fine grid results fairly closely.

For our next numerical tests we use 5×5 coarse-scale permeability field to generate the fine-scale 40×40 permeability field from posterior distribution. The coarse-scale permeability field is obtained using the upscaling procedure described previously and the precision parameter (see (2.11)) is chosen to be $\sigma^2 = 0.1$. In Figure 3.5 we plot the coarse-scale permeability field as well as the cross plot between the coarse-scale permeability fields obtained from the true and simulated fine scale permeability fields. Since for this case the coarse-scale permeability field is coarser compare to the previous case, 10×10 , the agreement between the true and simulated permeability fields is less accurate (see Figure 3.4). This is more noticeable from the Figure 3.6. In Figure 3.6 we plot the fractional flow curves generated for true and simulated permeability fields based on single-phase flow calculations, (3.1) as we did previously. Comparing Figure 3.3 and Figure 3.6 we can conclude that the fine-scale permeability field obtained from 10×10 coarse grid is more accurate than the fine-scale permeability field obtained from 5×5 coarse grid. In the same Figure, Figure 3.6, we also plot the fractional flow curve corresponding to 5×5 coarse grid block. This numerical result suggests that downscaling of the coarse-scale permeability is important for obtaining more accurate predictions. Finally, we present the numerical results that demonstrate that the downscaling based on coarse grids with higher precision can perform better than downscaling based on finer coarse grids with lower precisions. In the Figure 3.7 8×8 coarser grid with the precision $\sigma = 1$ is used. The obtained fine-scale permeability field is not accurate compare to that based on 5×5 coarse grid with high precision, $\sigma = 0.1$. This is more evident from the next Figure 3.8 where the fractional flow curves are compared. These results suggest that conditioning on the coarser grids with high precision can give more accurate results compare to the conditioning on the finer coarse grids with lower precision. Since the measured data, such as production data, represents the scales comparable to the inter-well distances the permeability obtained from the inversion at inter-well scales have higher precision and may provide more accurate predictions.

For our last numerical example we use the permeability field from [17] generated by a sequential Gaussian simulation and shown in Figure 3.11 (left Figure). The fine grid size is 128×64 and the coarse-scale data correspond to 15 injectors and 27 producers arranged in multiple five-spot patterns. There are two coarse-scales are involved, medium coarse-scale 64×32 which is obtained by a geometric averaging of the fine-scale permeability field and adding the error, $N(0, \sigma_1^2)$ with $\sigma_1^2 = 0.08$. The large scale coarse permeability field on 32×16 coarse grid is obtained by inversion of water cut ($1 - F$) responses at the 27 producing wells using streamline model [17]. The coarse-scale permeability fields and the locations of the sampling points

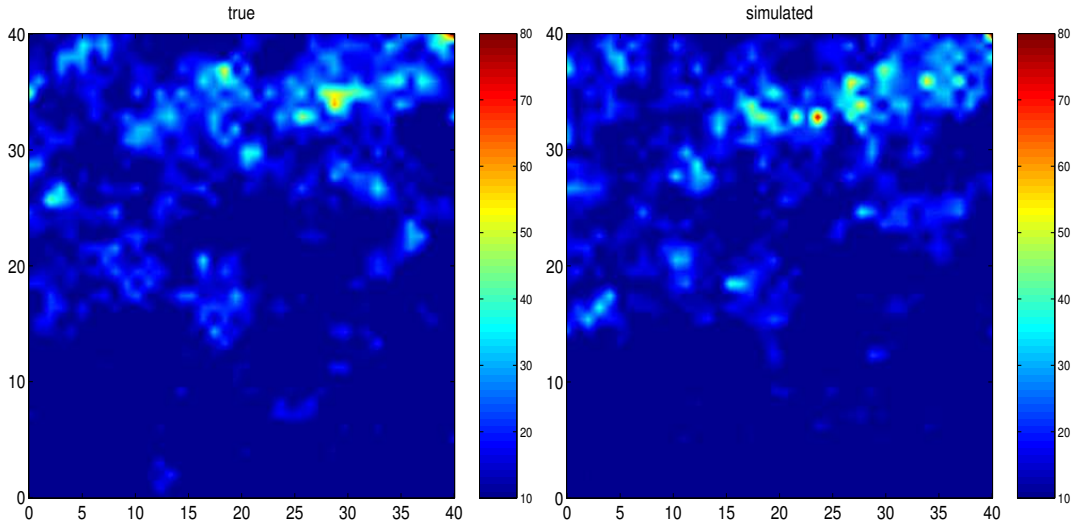


FIG. 3.1. Left figure is 40×40 true field and the right figure is 40×40 simulated field. 10×10 coarse-scale data is used for posterior distribution.

are plotted in Figures 3.9 and Figure 3.10. Compare with medium scale coarse-scale permeability field we use relatively large error variance, $\sigma_2^2 = 2$ for the large scale permeability field to represent its low precision. Using MCMC described above we simulate the fine-scale permeability fields that honor the medium scale permeability field on 64×32 grid, the large scale permeability field on 32×16 coarse grid, and the fine-scale conditioning points. A realization of the fine field sampled from the posterior distribution is shown in Figure 3.11. In Figure 3.12 a realization of the fine-scale permeability field conditioned only on the large scale permeability data on 32×16 and fine-scale conditioning points is shown. Comparing Figure 3.11 and 3.12 we see that the agreement is worse if we only condition on the large scale data. In the Figure 3.13 and Figure 3.14 some representative numerical results for water cut for various wells are presented. We see from these Figures that the results corresponding to 2 scale data (the fine-scale permeability field conditioned to the coarse-scale 32×16 data and some sampling points) is worse than those corresponding to 3 scale data (the fine-scale permeability field conditioned to the coarse-scale 32×16 and 64×32 data and some sampling points). However, water cut results with 2 scale data are predicted fairly accurately in most wells.

4. Conclusions and Future Work. In this paper we propose a method for reconstructing the fine scale permeability field from a coarse-scale permeability data and some sampling points. The upscaling methods have been used in the calculation of the posterior distribution. Since the upscaling operators are non-local and non-explicit, Markov Chain Monte Carlo methods are used to draw samples from the posterior distribution. The proposed method allows us to integrate as many scales as required by the available data. Moreover, using the proposed method we can take into account non-linear interaction between scales and uncertainties in the prior models. Currently, we are developing sampling techniques that are more suitable to the upscaling procedures and studying the applications of Langevin algorithms. We are also considering the use of more accurate upscaling methodologies such as local-global upscaling methods [3].

Appendix A. The effects of upscaling errors on posterior distribution.

In this Appendix we study the effects of the errors in the computation of upscaled permeability on the posterior distribution. We start with the description of the effective permeability for random homogeneous fields and will only consider one coarse block. Let (Ω, Σ, μ) be a probability space. A random homogeneous field is a measurable function on Ω and $f(T(x)\omega)$ are realizations of the random field. The realizations are well-defined measurable functions on R^d for almost all $\omega \in \Omega$. Consider a d dimensional dynamical system on Ω , $T(x) : \Omega \rightarrow \Omega$, $x \in R^d$, that satisfies the following conditions: 1) $T(0) = I$, and $T(x+y) = T(x)T(y)$; 2) $T(x) : \Omega \rightarrow \Omega$ preserve the measure μ on Ω ; 3) For any measurable function $f(\omega)$ on Ω , the function

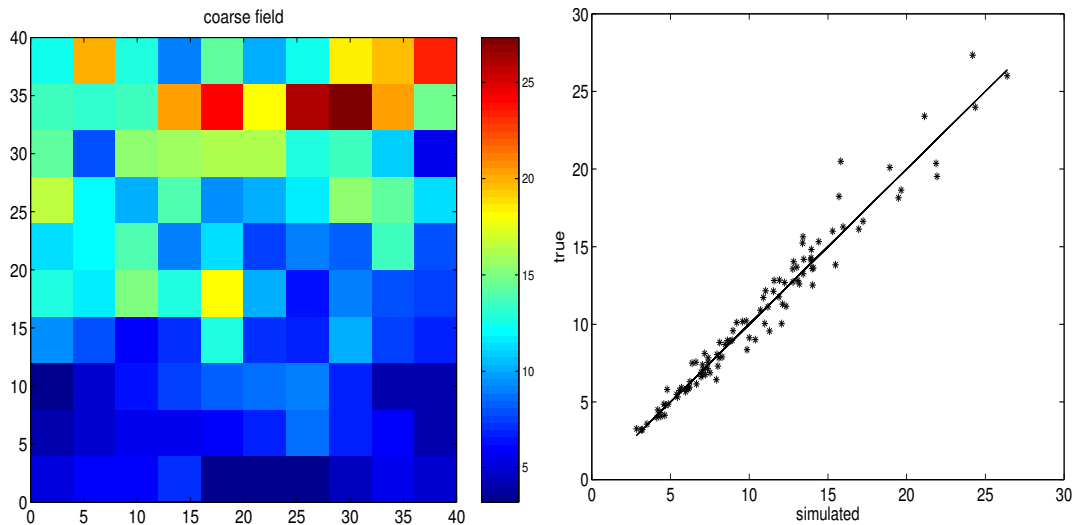


FIG. 3.2. The coarse 10×10 field corresponding to 40×40 true field (left plot). The cross-plot of coarse permeability fields corresponding to the true and simulated permeability fields.

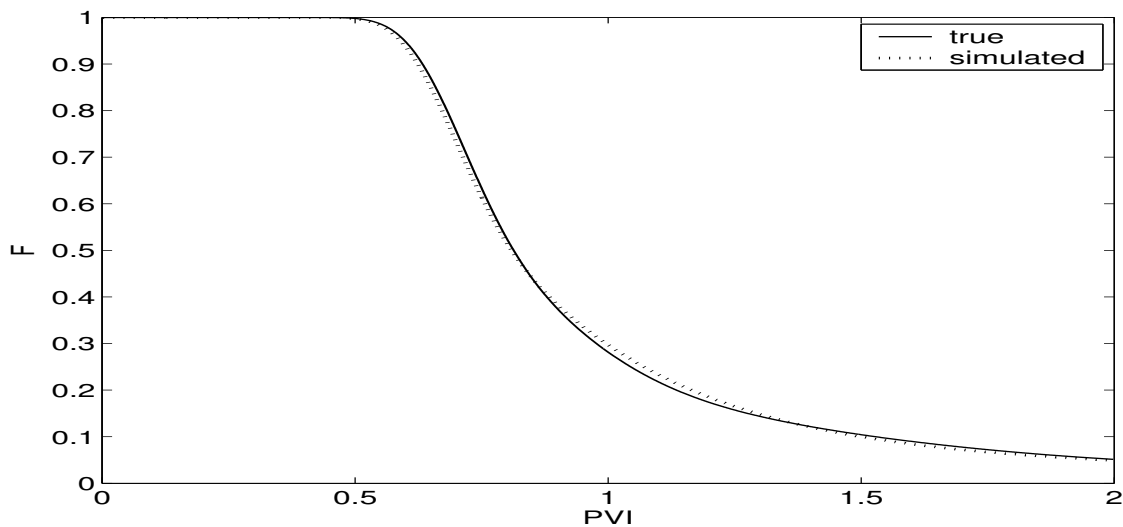


FIG. 3.3. Fractional flow curves corresponding to the true and simulated fields. 10×10 coarse-scale data is used for posterior distribution.

$f(T(x)\omega)$ defined on $R^d \times \Omega$ is also measurable (see [15, 19]). Let $L^p(\Omega)$ denote the space of all p -integrable functions on Ω . Then $U(x)f(\omega) = f(T(x)\omega)$ defines a d -parameter group of isometries in the space $L^p(\Omega)$, and $U(x)$ is strongly continuous [15, 18]. Denote by $\langle \cdot \rangle$ the mean value over Ω ,

$$\langle f \rangle = \int_{\Omega} f(\omega) d\mu(\omega) = E(f).$$

The relation between the standard definition of random homogeneous fields and the one introduced here can be found e.g., [15].

Denote by D_{ω}^i the generator of $U(x)$ along i th coordinate direction, i.e.,

$$D_{\omega}^i = \lim_{\delta \rightarrow 0} \frac{f(T(x_i)\omega) - f(\omega)}{\delta}.$$

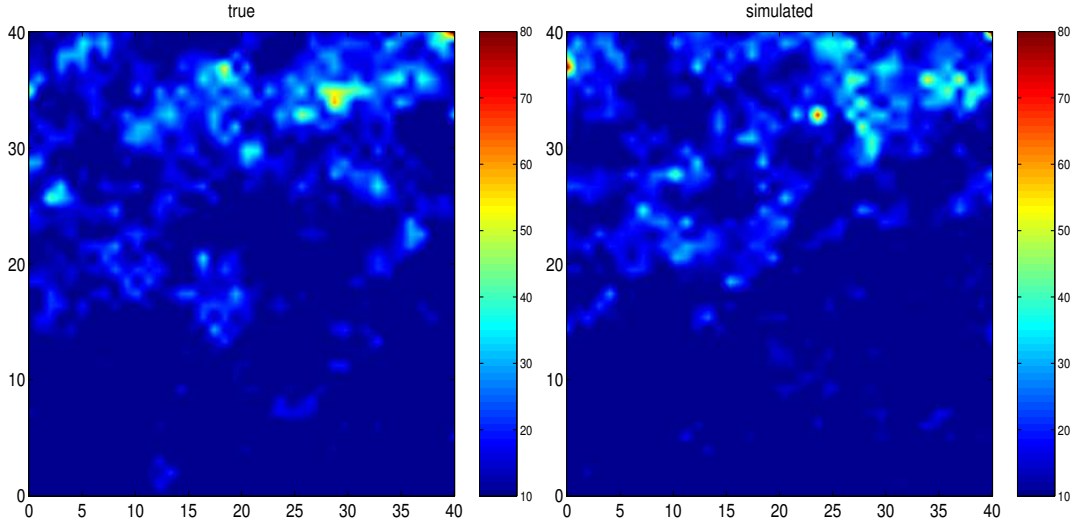


FIG. 3.4. Left figure is 40×40 true field and the right figure is 40×40 simulated field. 5×5 coarse-scale data is used for posterior distribution.

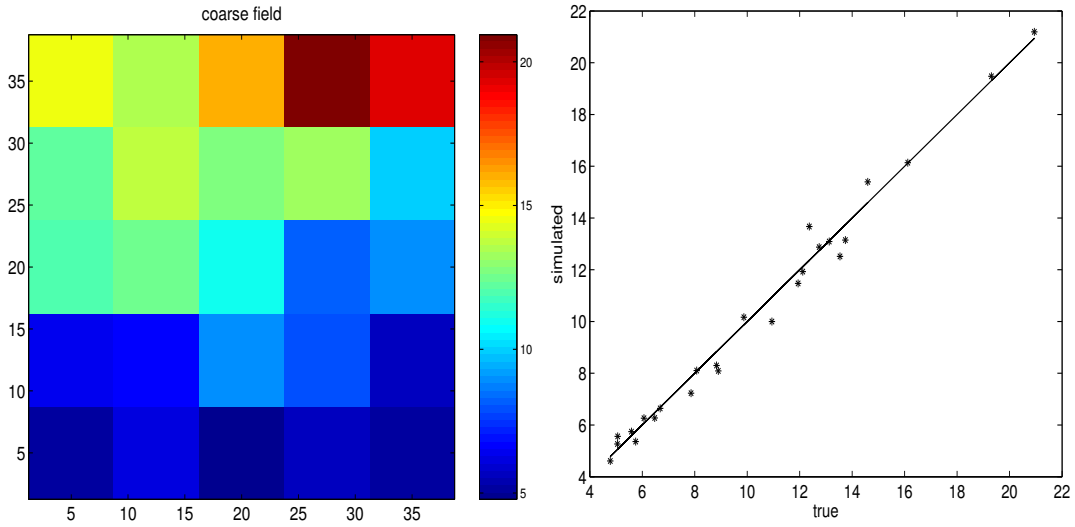


FIG. 3.5. The coarse 5×5 field corresponding to 40×40 true field (left plot). The cross-plot of coarse permeability fields corresponding to the true and simulated permeability fields.

The domains ∂_i of D_ω^i are dense in $L^2(\Omega)$, and the intersection of all D_ω^i is also dense. Next we introduce ergodicity. A subset $A \in \Sigma$ is invariant if $T(x)A = A$ for any $x \in R^d$. A dynamical system is said to be ergodic if for any invariant set $A \in \Sigma$ we have either $P(A) = 1$ or $P(A) = 0$. Further following [15, 18] we define potential and solenoidal fields. A vector field $f \in L^p(\Omega)$ ($p > 1$) is said to be potential (or solenoidal respectively) if its generic realization $f(T_x\omega)$ is a *potential* (or *solenoidal* respectively) vector field in R^d . Denote by $L_{pot}^p(\Omega)$ (respectively $L_{sol}^p(\Omega)$) the subspace of $L^p(\Omega)$ that consists of all potential (respectively solenoidal) vector fields. Introduce the following notations:

$$V_{pot}^p = \{f \in L_{pot}^p(\Omega), \langle f \rangle = 0\}, \quad V_{sol}^p = \{f \in L_{sol}^p(\Omega), \langle f \rangle = 0\}.$$

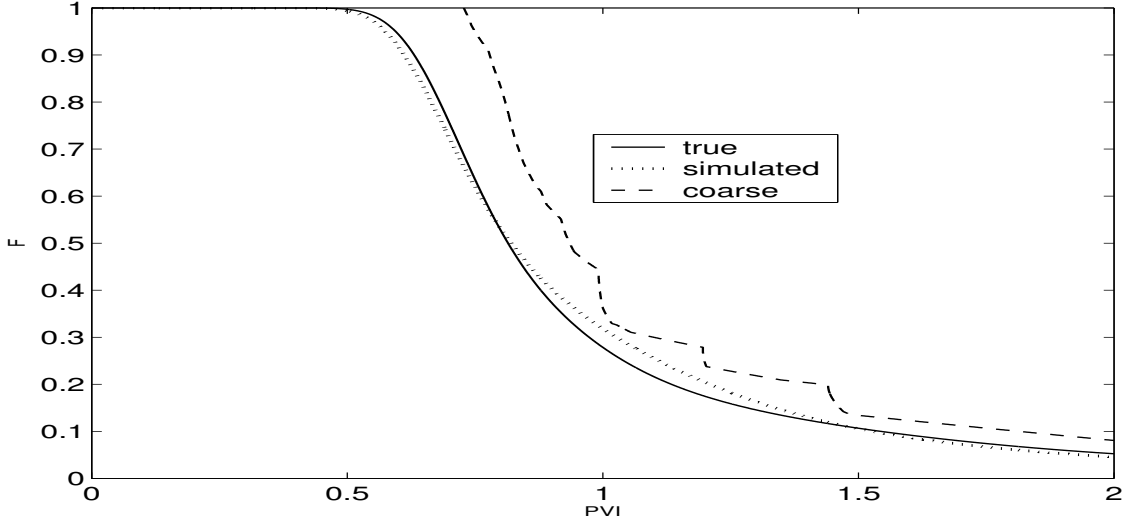


FIG. 3.6. Fractional flow curves corresponding to the true and simulated fields. 5×5 coarse-scale data is used for posterior distribution.

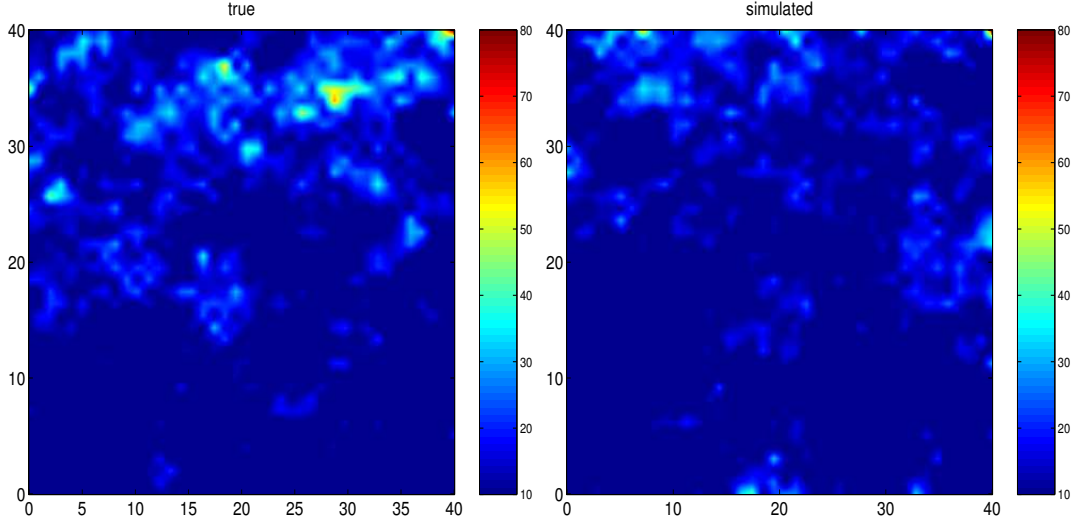


FIG. 3.7. Left figure is 40×40 true field and the right figure is 40×40 simulated field simulated field. 8×8 coarse-scale data with $\sigma = 1$ is used for posterior distribution.

The following properties are known (see [18], page 138):

$$L_{pot}^p(\Omega) = V_{pot}^p \oplus R^d, \quad L_{sol}^p(\Omega) = V_{sol}^p \oplus R^d, \quad L_{sol}^q(\Omega) = (V_{pot}^p)^\perp, \quad L_{pot}^q(\Omega) = (V_{sol}^p)^\perp.$$

Consider

$$A_\epsilon = \frac{\partial}{\partial x_i} k_{ij}(T(x/\epsilon)\omega) \frac{\partial}{\partial x_j},$$

where $c|\xi|^2 \leq k_{ij}(\omega)\xi_i\xi_j \leq C|\xi|^2$. It is known that the homogenized coefficient is defined by [15, 2]

$$k^*(\omega)\eta = E[a(\omega)(\eta + v_\eta(\omega)) | \sigma_{inv}]$$

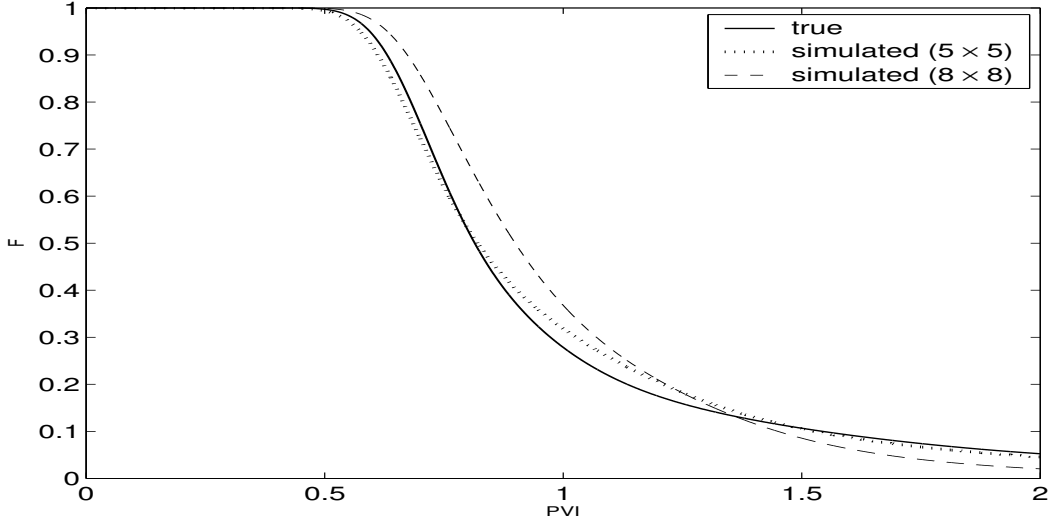


FIG. 3.8. Fractional flow curves corresponding to the true and simulated fields with. Solid line designates the fractional flow curve corresponding to the true permeability field, dotted line designates the fractional flow curve corresponding 5×5 coarse grid with $\sigma = 0.1$ and dashed line designates the fractional flow curve corresponding to 8×8 coarse-scale data with $\sigma = 1$.

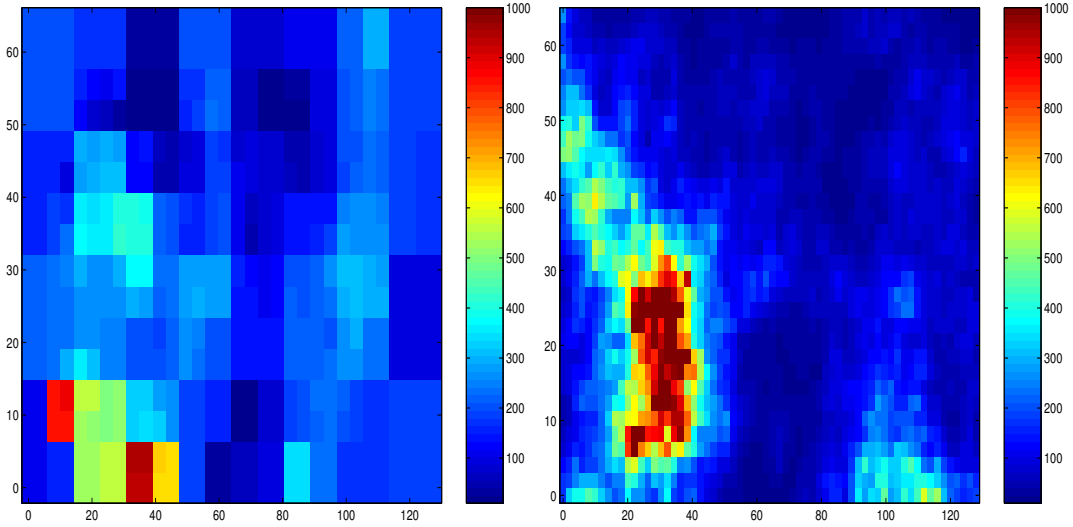


FIG. 3.9. The left plot is the 32×16 field corresponding to the medium scale permeability field. The right plot is the 64×32 field corresponding to the large scale permeability field.

where $v_\eta(\omega) \in L^2_{pot}(\Omega)$ is the solution of

$$k(\omega)(\eta + v_\eta(\omega)) \in L^2_{sol}(\Omega),$$

and

$$\sigma_{inv} = \{A \in \Sigma | T(x)A = A \text{ for all } x \in R^d\}.$$

The approximation for k^* is obtained from the solution of the local problem as it is described before,

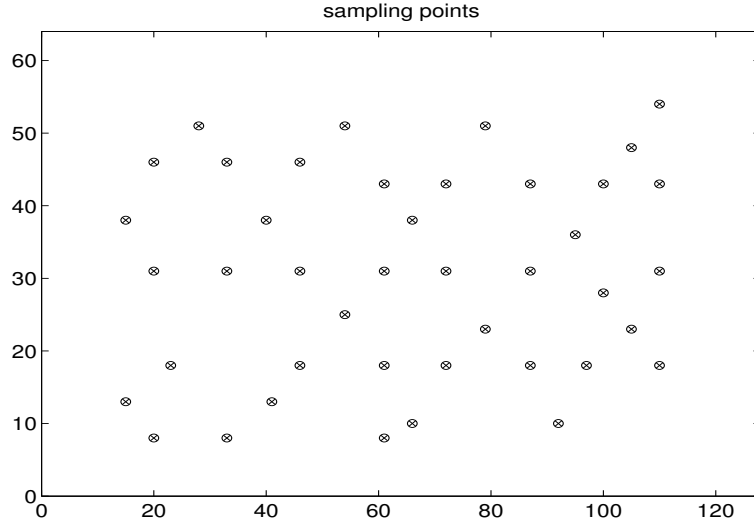


FIG. 3.10. The locations of the sampling points used for simulation of 128×64 permeability field

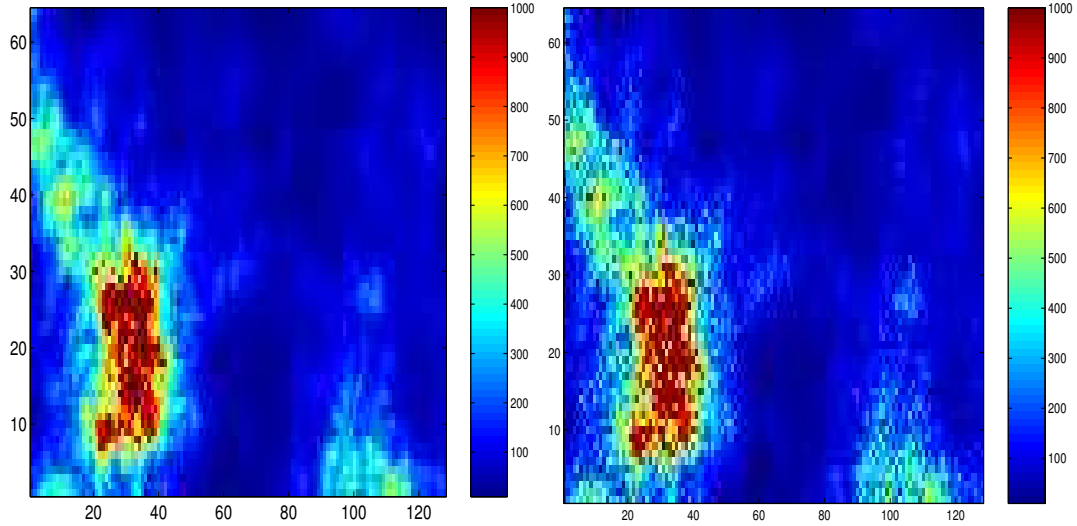


FIG. 3.11. The 128×64 field (right plot) corresponds to the simulated fine-scale permeability obtained from 32×16 coarse-scale data from the inversion of the production data and 64×32 averaged data. Left figure is 128×64 true permeability field.

i.e.,

$$(\tilde{k}_\epsilon^*(\omega)e_m, e_l) = \frac{1}{|K|} \int_K (k(T(x/\epsilon)\omega) \nabla v_\epsilon, e_l) dx,$$

where v_ϵ is the solution of the local problem described previously. Using G-convergence of arbitrary solution ([15]) one can easily show that (see [2])

$$\tilde{k}_\epsilon^* \rightarrow k^* \quad (\text{A.1})$$

μ -a.s.

Under more restrictive assumption, such as uniform mixing, one can obtain explicit convergence rate.

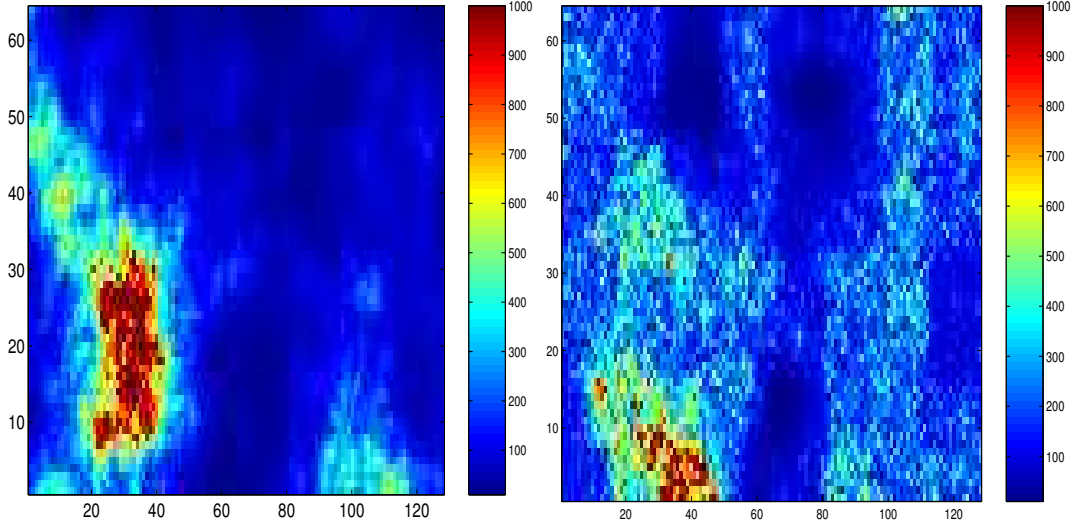


FIG. 3.12. The 128×64 field (right plot) corresponds to the simulated fine-scale permeability obtained from 32×16 coarse-scale data from the inversion of the production data. Left figure is 128×64 true permeability field.

We recall the definition of strong mixing. Define

$$m(s) = \sup_{A, B \in \mathcal{R}^d, \text{dist}(A, B) \geq s} \sup_{A \in \sigma_A, B \in \sigma_B} |P(A \cap B) - P(A)P(B)|.$$

We assume that $m(s)$ defined by the parameters of the problem satisfies

$$m(s) \leq \frac{c}{(1+s)^\kappa}$$

where $\kappa > 0$. Under strong mixing assumption it can be shown that (see (see [2]))

$$E|\tilde{k}_\epsilon^* - k^*|^2 \leq C\epsilon^\beta. \quad (\text{A.2})$$

Next we study the convergence of the posterior distributions assuming strictly stationarity of the coefficients. The convergence of posterior distributions in "stronger sense" can be shown under strong-mixing conditions. The posterior distribution corresponding to the approximate upscaled permeability is given by

$$P(k_\epsilon | \tilde{k}_\epsilon^*) = P(\tilde{k}_\epsilon^* | k_\epsilon)P(k_\epsilon) / P(\tilde{k}_\epsilon^*).$$

For further analysis we re-write the posterior distribution in the following form

$$P_\epsilon(k_\epsilon | k) = P_\epsilon(k | k_\epsilon)P(k_\epsilon) / P(k),$$

where

$$P_\epsilon(k | k_\epsilon) = \frac{1}{\sigma_2 \sqrt{2\pi}} \exp\left(-\frac{1}{2\sigma_2^2}(k - \mathcal{L}(k_\epsilon))^2\right).$$

Our first goal is to show that $P_\epsilon(k | k_\epsilon)$ converges to $P(k | k_\epsilon)$ which is given by

$$P(k | k_\epsilon) = \frac{1}{\sigma_2 \sqrt{2\pi}} \exp\left(-\frac{1}{2\sigma_2^2}(k - k^*)^2\right).$$

Taking the ratio of these two we have

$$\frac{P_\epsilon(k | k_\epsilon)}{P(k | k_\epsilon)} = \exp\left(-\frac{1}{2\sigma_2^2}(\mathcal{L}(k_\epsilon) - k^*)(\mathcal{L}(k_\epsilon) + k^*)\right) \exp\left(-\frac{k}{\sigma_2^2}(\mathcal{L}(k_\epsilon) - k^*)\right) \quad (\text{A.3})$$

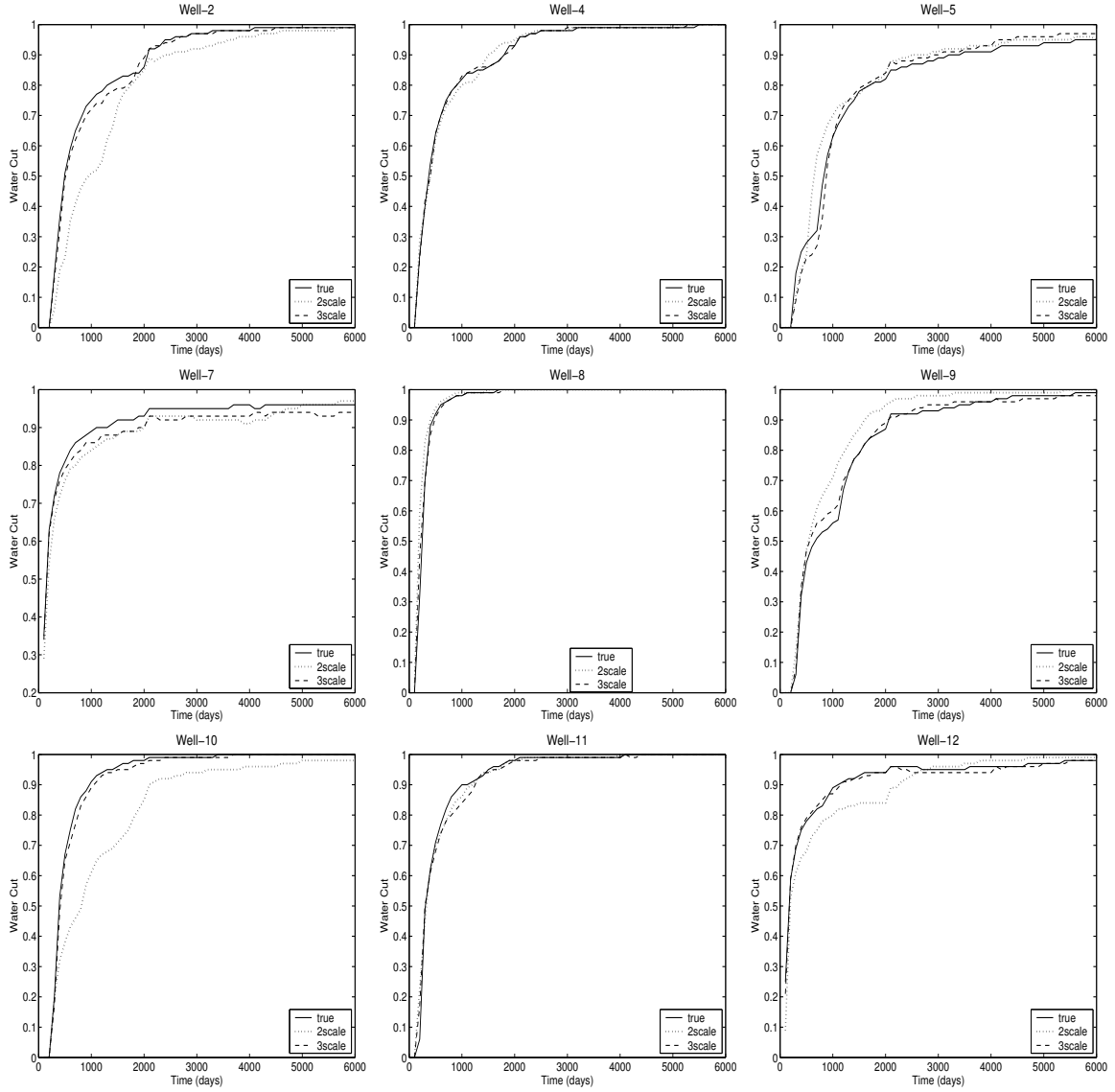


FIG. 3.13. Water cut results corresponding to 2 scale data (fine-scale data conditioned to 32×16 coarse-scale data and the sampling points) and 3 scale data (fine-scale data conditioned to both 32×16 and 64×32 coarse-scale data and the sampling points)

It follows from general G -convergence results [15] that k^* is bounded ($c|\xi|^2 \leq k_{ij}^* \xi_i \xi_j \leq C|\xi|^2$) because k_ϵ is bounded. Similarly, we can show that $\mathcal{L}(k_\epsilon)$ is uniformly bounded. Thus

$$\frac{P_\epsilon(k|k_\epsilon)}{P(k|k_\epsilon)} \leq \exp(-C(\mathcal{L}(k_\epsilon) - k^*))$$

for some positive C assuming that k belongs to a compact set. Next due to (A.1) we have

$$\mathcal{L}(k_\epsilon) - k^* \rightarrow 0$$

μ -a.s. The latter implies that $P_\epsilon(k|k_\epsilon) - P(k|k_\epsilon) \rightarrow 0$ for each k_ϵ μ -a.s. Moreover, using Lebesgue's dominated convergence theorem one can easily show that $P_\epsilon(k) \rightarrow P(k)$ as $\epsilon \rightarrow 0$ μ -a.s. Thus, we have shown that

$$P(k_\epsilon|\tilde{k}_\epsilon^*) - P(k_\epsilon|k^*) \rightarrow 0$$

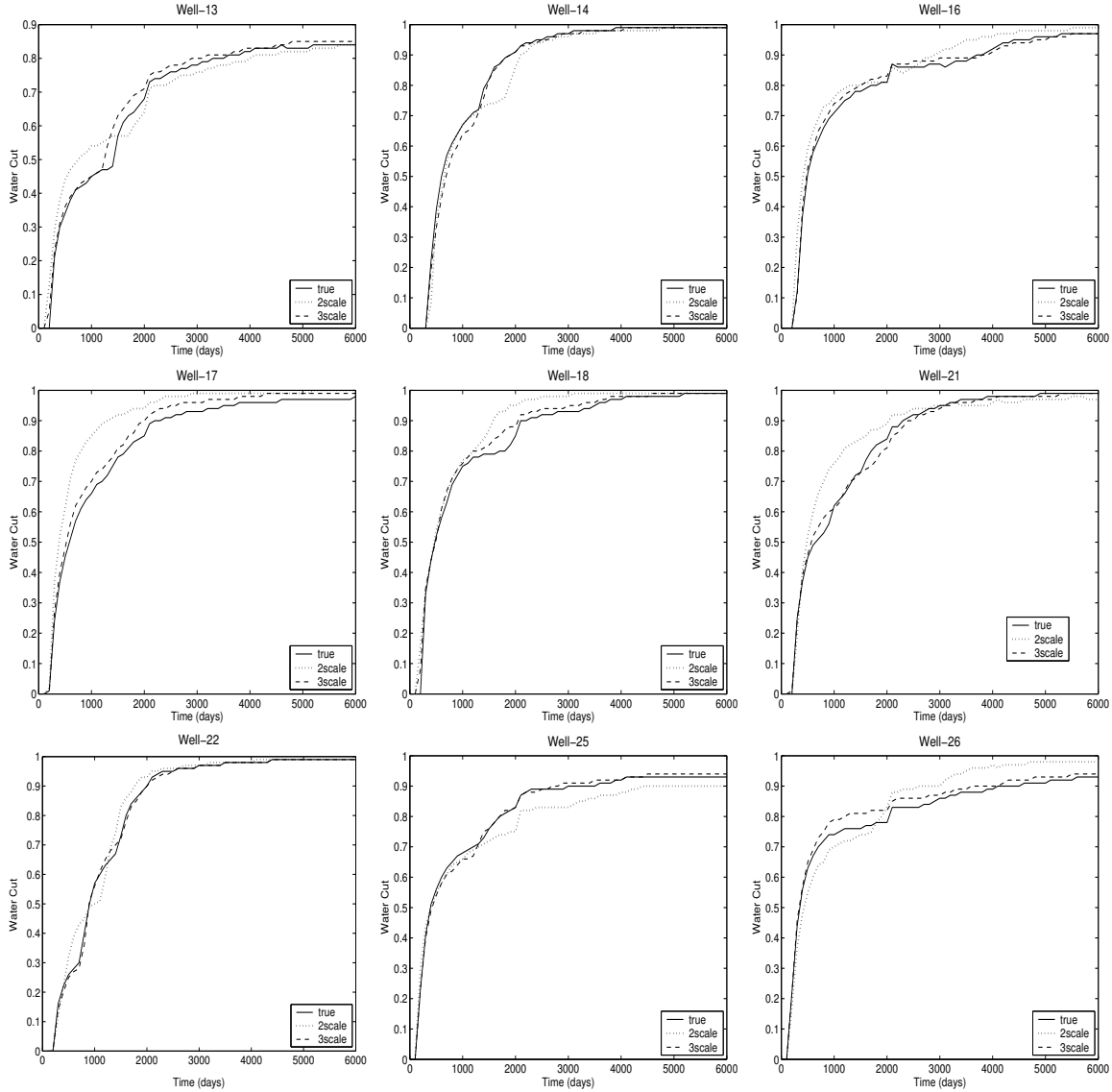


FIG. 3.14. Water cut results corresponding to 2 scale data (fine-scale data conditioned to 32×16 coarse-scale data and the sampling points) and 3 scale data (fine-scale data conditioned to both 32×16 and 64×32 coarse-scale data and the sampling points)

as $\epsilon \rightarrow 0$ μ -a.s. under the assumption that k_ϵ is a compact set.

REFERENCES

- [1] R. BEHRENS AND T. TRAN, *Incorporating seismic data of intermediate vertical resolution into 3d reservoir models*. SPE 49143 paper presented at the 1998 SPE Annual Technical Conference and Exhibition, New Orleans, LA, October 4-7.
- [2] A. BOURGEAT AND A. PIATNITSKI, *Approximations of effective coefficients in stochastic homogenization*. preprint.
- [3] Y. CHEN, L. J. DURLOFSKY, M. GERRITSEN, AND X. H. WEN, *A coupled local-global upscaling approach for simulating flow in highly heterogeneous formations*, Advances in Water Resources, 26 (2003), pp. 1041–1060.
- [4] G. CHRISTAKOS, *Random Field Models in Earth Sciences*, Academic Press, San Diego, 1992.
- [5] C. DEUTSCH, S. SRINIVASAN, AND Y. MO, *Geostatistical reservoir modeling accounting for precision and scale of seismic data*. SPE 36497 paper presented at the 1996 SPE Annual Technical Conference and Exhibition, Denver, Colorado, October 6-9.

- [6] P. DOYEN, D. PSAILA, L. DEN BOER, AND D. JANS, *Reconciling data at seismic and well log scales in 3-d earth modeling*. SPE 38698 paper presented at the 1997 SPE Annual Technical Conference and Exhibition, San Antonio, TX, October 5-8.
- [7] O. DUBRULE, *Estimating or Choosing a Geostatistical Model*, Kluwer Academic Publishers, Dordrecht, The Netherlands, 1994.
- [8] L. J. DURLOFSKY, *Numerical calculation of equivalent grid block permeability tensors for heterogeneous porous media*, Water Resour. Res., 27 (1991), pp. 699–708.
- [9] ———, *Coarse scale models of two phase flow in heterogeneous reservoirs: Volume averaged equations and their relationship to the existing upscaling techniques*, Computational Geosciences, 2 (1998), pp. 73–92.
- [10] Y. EFENDIEV AND L. DURLOFSKY, *Accurate subgrid models for two-phase flow in heterogeneous reservoirs*. SPE 79680, to appear in SPE Journal of Reservoir Simulation.
- [11] ———, *Generalized convection-diffusion model for subgrid transport in porous media*, SIAM Multiscale Modeling and Simulation, 1(3) (2003), pp. 504–526.
- [12] Y. R. EFENDIEV AND L. J. DURLOFSKY, *Numerical modeling of subgrid heterogeneity in two phase flow simulations*, Water Resour. Res., 38(8) (2002), p. 1128.
- [13] P. FRYKMAN AND C. DEUTSCH, *Geostatistical scaling laws applied to core and log data*. SPE 56822 paper presented at the 1999 SPE Annual Technical Conference and Exhibition, Houston, TX, October 3-6.
- [14] W. GILKS, S. RICHARDSON, AND D. SPEGELHALTER, *Markov Chain Monte Carlo in Practice*, Chapman and Hall/CRC, London, 1996.
- [15] V. V. JIKOV, S. M. KOZLOV, AND O. A. OLEINIK, *Homogenization of differential operators and integral functionals*, Springer-Verlag, New York, 1994.
- [16] S. H. LEE, A. MALALLAH, A. DATTA-GUPTA, AND D. HIGDON, *Multiscale data integration using Markov random fields*. SPE Annual Technical Conference and Exhibition, Dallas, TX, October, 2000. SPE paper number 63066.
- [17] S. H. LEE, A. MALALLAH, A. DATTA-GUPTA, AND D. HIGDON, *Multiscale data integration using markov random fields*, SPE Reservoir Evaluation and Engineering. February 2002.
- [18] A. PANKOV, *G-convergence and homogenization of nonlinear partial differential operators*, Kluwer Academic Publishers, Dordrecht, 1997.
- [19] G. PAPANICOLAOU AND S. R. S. VARADHAN, *Boundary value problems with rapid oscillating random coefficients*, Seria Colloquia Mathematica Societatis Janos Bolyai, 27 (1981), pp. 835–873.
- [20] X. H. WU, Y. R. EFENDIEV, AND T. Y. HOU, *Analysis of upscaling absolute permeability*, Discrete and Continuous Dynamical Systems, Series B, 2 (2002), pp. 185–204.
- [21] W. XU, T. TRAN, R. SRIVASTAVA, AND C. DEUTSCH, *Integrating seismic data in reservoir modeling: The collocated cokriging approach*. SPE 24742 paper presented at the 1992 SPE Annual Technical Conference and Exhibition, Washington, DC, October 4-7.
- [22] G. XUE AND A. DATTA-GUPTA, *A new approach to seismic data integration during reservoir characterization using optimal nonparametric transformations*. SPE 36500 paper presented at the 1996 SPE Annual Technical Conference and Exhibition, Denver, CO, October 6-9.